

Article

Synthesis of Al₂Ca Dispersoids by Powder Metallurgy Using a Mg–Al Alloy and CaO Particles

Junji Fujita ^{1,2,*}, Junko Umeda ³ and Katsuyoshi Kondoh ³

¹ HI-LEX CORPORATION, 1-12-28 Sakaemachi, Takarazuka-City, Hyogo 665-0845, Japan

² Graduate School of Engineering, Osaka University, 2-1 Yamadaoka, Suita, Osaka 565-0871, Japan

³ Joining and Welding Research Institute, Osaka University, 11-1 Mihogaoka, Ibaragi, Osaka 567-0047, Japan; umedaj@jwri.osaka-u.ac.jp (J.U.); kondoh@jwri.osaka-u.ac.jp (K.K.)

* Correspondence: jun-fujita@hi-lex.co.jp; Tel.: +81-797-852-571

Received: 1 June 2017; Accepted: 22 June 2017; Published: 28 June 2017

Abstract: The elemental mixture of Mg-6 wt %Al-1 wt %Zn-0.3 wt %Mn (AZ61B) alloy powder and CaO particles was consolidated by an equal-channel angular bulk mechanical alloying (ECABMA) process to form a composite precursor. Subsequently, the precursor was subjected to a heat treatment to synthesize fine Al₂Ca particles via a solid-state reaction between the Mg–Al matrix and CaO additives. Scanning electron microscopy-energy-dispersive spectroscopy (SEM-EDS) and electron probe micro-analysis on the precursor indicated that 4.7-at % Al atoms formed a supersaturated solid solution in the α -Mg matrix. Transmission electron microscopy-EDS and X-ray diffraction analyses on the AZ61B composite precursor with 10-vol % CaO particles obtained by heat treatment confirmed that CaO additives were thermally decomposed in the Mg–Al alloy, and the solid-soluted Ca atoms diffused along the α -Mg grain boundaries. Al atoms also diffused to the grain boundaries because of attraction to the Ca atoms resulting from a strong reactivity between Al and Ca. As a result, needle-like (Mg,Al)₂Ca intermetallics were formed as intermediate precipitates in the initial reaction stage during the heat treatment. Finally, the precipitates were transformed into spherical Al₂Ca particles by the substitution of Al atoms for Mg atoms in (Mg,Al)₂Ca after a long heat treatment.

Keywords: magnesium alloys; powder metallurgy; composite materials; microstructure; phase transformation; transmission electron microscopy

1. Introduction

Magnesium alloys are remarkably lightweight due to the low density of Mg (~1.74 g/cm³). Their application to structural components in automobiles can improve fuel consumption [1–4]. In particular, the weight reduction of engine blocks and transmission cases used at elevated temperatures (120–200 °C) is very important [4–6]. However, the tensile strength of Mg alloys drastically decreases at elevated temperatures. This prevents their widespread use in the automotive industry [5–7]. Therefore, it is necessary to improve the heat resistance of Mg alloys. Previous studies have reported that the addition of calcium to Mg–Al alloys improved the creep resistance at 200 °C by the formation of Al₂Ca or (Mg,Al)₂Ca intermetallic compounds around the α -Mg grain boundaries [8–10]. This is because these network-structured compounds prevented both the deformation of α -Mg grains and grain boundary sliding at elevated temperatures. On the other hand, these network-structured compounds potentially cause grain boundary fractures. Fine dispersed particles of intermetallic compounds are more effective to improve the yield stress of Mg alloys via pinning effects.

In the present study, CaO particles are employed as raw materials to disperse fine Al₂Ca particles in an α -Mg matrix via a solid-state reaction between CaO particles and the Mg–Al alloy. The conventional Mg–Al alloys reinforced with fine Al₂Ca particles are expected to demonstrate both

excellent yield stress by pinning effects and high cost performance because of the use of inexpensive CaO particles as raw materials. However, from a thermodynamic point of view, an Ellingham diagram of the oxide formation [11] indicates that CaO reduction by Mg never occurs in the solid state (up to 650 °C). Therefore, the CaO raw particles should remain in the cast Mg material. In contrast, our previous study [12] reported that CaO reduction with Al₂Ca and MgO formation occurred in the Mg-6 wt %Al-1 wt %Zn-0.3 wt %Mn (AZ61B) alloy instead of pure Mg because the change in the standard free energy became negative. As a result, Al₂Ca phases were synthesized in the AZ61B alloy. Furthermore, CaO particles homogeneously dispersed in the α-Mg matrix contributed to forming the Al₂Ca fine particles via a solid-state synthesis. Another study [13] reported that Mg-6 wt %Al alloy (AM60) powder composites with CaO additive particles demonstrated a higher creep resistance at 175 °C than those of the ADC12 aluminum alloy. This is because these composites were reinforced with Al₂Ca fine dispersoids formed via a solid-state reaction between the CaO particles and the AM60 alloy.

Nevertheless, the reaction mechanism for CaO reduction in Mg–Al alloys is not yet clear. For example, a previous study [12] revealed that needle-like intermetallics were formed as intermediate precipitates from the solid-state reaction, as shown in Figure 1. However, the crystal structure was not completely identified. Furthermore, the reaction process of the Al₂Ca synthesis was also not clear. The same study [12] suggests that the progress of this reaction is governed by the diffusion behavior of Al atoms to CaO particles. This is because Al₂Ca formation was more clearly detected after heat treatment at higher temperatures as shown in Figure 2 [12]. By contrast, Figure 2 also reveals that the progress of the Al₂Ca synthesis was promoted by the increase of CaO additive particles. In particular, no Al₂Ca was detected in the Mg–Al–CaO precursor with 2.5-vol % CaO particles. This reason cannot be well-explained by only the diffusion behavior of Al atoms because all of the CaO particles should contact the Al atoms solid-soluted in the α-Mg matrix during the heat treatment.

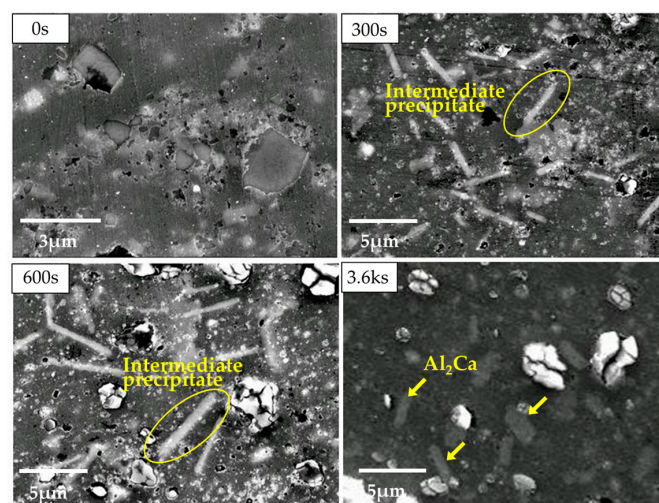


Figure 1. Scanning electron microscopy (SEM) observation on the Mg–Al–CaO precursors with 10-vol % CaO particles after the heat treatment at 500 °C for 0 s, 300 s, 600 s and 3.6 ks.

In this study, the synthesis mechanism of Al₂Ca intermetallic compounds via a reaction of CaO additives dispersed in an AZ61B composite precursor during heat treatment was investigated in detail by scanning electron microscopy (SEM), transmission electron microscopy (TEM), electron probe micro-analysis (EPMA), and X-ray diffraction (XRD) analysis. The atomic distribution of Mg, Al, and Ca was determined by TEM-energy-dispersive spectrometry (EDS) and XRD analysis using the AZ61B composite precursor with 10-vol % CaO particles at the initial stage of the heat treatment. The synthesis of (Mg,Al)₂Ca intermediate precipitates was also detected through crystal structure analysis by XRD and TEM-EDS analysis.

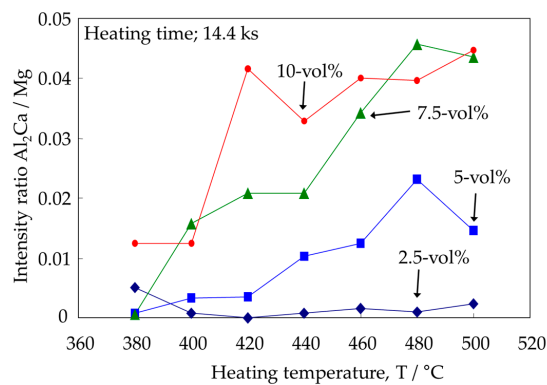


Figure 2. Dependence of X-ray diffraction (XRD) peak intensity ratio of Al_2Ca and Mg peaks on heating temperature of AZ61B powder precursors with various contents of CaO particles.

2. Materials and Methods

2.1. Preparation of AZ61B Precursors Containing CaO Particles

AZ61B chips machined from their original cast ingot (Al; 6.41, Zn; 1.02, Mn; 0.28, Si; 0.02, Fe; 0.004, Cu; 0.002, Ni; 0.0007, Mg; Bal./mass %) were employed as raw materials. They had a mean particle size of 1.38 mm as measured by a particle size analyzer (LA-950, HORIBA, Kyoto, Japan). CaO particles for use as additives, having a mean particle size of 2.3 μm , were prepared from CaO blocks with a purity of 98% or more via mechanical fragmentation using a ball milling process. The elemental mixtures of the AZ61B chips and CaO particles were mixed by rocking mill equipment (RM-05S, Seiwa Giken Co., Hiroshima, Japan) and used as the starting materials. The content of the CaO additives was 10-vol %. It is effective to disperse CaO additive particles homogeneously in the Mg–Al alloy matrix in order to form Al_2Ca fine particles via a solid-state synthesis during the heat treatment. Therefore, a severe plastic working was applied to the AZ61B green compacts containing CaO particles by an equal-channel angular bulk mechanical alloying (ECABMA) process [14], where cold compaction and extrusion within a channel bent were alternately carried out in the die, as illustrated in Figure 3. The maximum compaction pressure was 611 MPa. The ECABMA process was repeated 50 times in total resulting in the homogeneous dispersion of the CaO additive particles in the AZ61B alloy chip matrix. This process was also effective for the mechanical breakage of the MgO surface oxide films of the AZ61B chips, and resulted in the formation of newly created Mg active surfaces of the chips that directly came into contact with the CaO particles. The green compact billet (Mg–Al–CaO precursor) prepared by the above process had a 35 mm diameter and an 80 mm length.

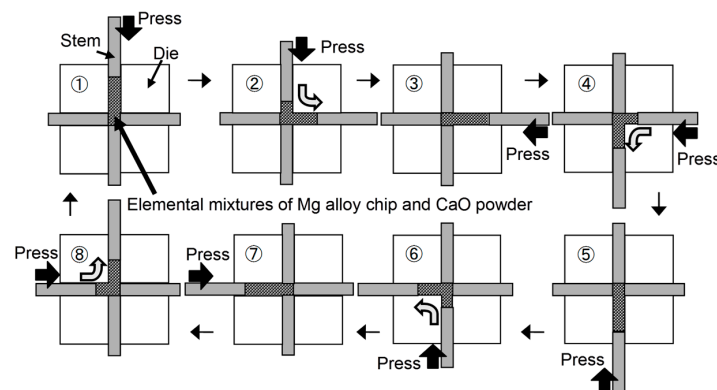


Figure 3. Schematic illustration of one cycle of equal channel angular bulk mechanical alloying (ECABMA) process used in fabrication of Mg alloy powder precursor containing CaO particles.

2.2. Heat Treatment of AZ61B Composite Precursor with CaO Particles

A heat treatment at 500 °C in an argon gas atmosphere was applied to the precursor in order to investigate the reaction behavior between the AZ61B matrix and the CaO particles in the initial stage. The heating time at 500 °C was 300 s. For the investigation of the Al atom distribution in the AZ61B matrix, the aging heat treatment of the AZ61B precursor with no CaO particle was conducted at 200 °C for 86.4 ks in vacuum.

2.3. Microstructural Analysis

A field emission scanning electron microscope (JSM-6500F, JEOL, Tokyo, Japan) equipped with an energy-dispersive X-ray spectrometer (EX-64175 JMU, JEOL) was used to investigate the microstructures of the AZ61B powder precursor with no CaO particle. The chemical composition of the Mg–Al matrix was investigated by an electron probe micro-analyzer (EPMA, JXA-8530F, JEOL). The number of the EPMA measurement point was 15, and the mean value was calculated. A transmission electron microscope (JEM-2100F, JEOL) equipped with an energy dispersive X-ray spectrometer (EX-37001, JEOL) was used to investigate the microstructures of the heat treated precursors. X-ray diffraction analysis (XRD-6100, Shimadzu, Kyoto, Japan) was used to clarify the crystal structure of the α -Mg matrix and identify the intermediate precipitates.

3. Results and Discussion

3.1. Microstructural and Compositional Analysis on the AZ61B Matrix with No CaO Particle

The microstructures and compositions of the AZ61B powder precursor with no CaO particles were investigated. As shown in Figure 4, SEM on the AZ61B powder precursor after the ECABMA process suggests that coarse β -phases ($\text{Mg}_{17}\text{Al}_{12}$), having a particle size of 2–10 μm , and Al_6Mn phases were observed in the α -Mg matrix. Table 1 shows the EPMA analysis results for the α -Mg matrix in the precursor. The mean value of the Al composition in the α -Mg matrix was 4.7-at % (5.17-wt %). This means that 80.7% of the entire Al content (6.41-wt %) from the original AZ61B chips was solid-soluted in the α -Mg matrix. The remaining 19.3% contributed to the formation of β -phases and/or Al_6Mn compounds. The Mg–Al binary phase diagram [15] suggests that a solid solubility limit of Al into the α -Mg phase is 1-at % or lower below 100 °C. Therefore, the above 4.7-at % Al elements existed as a supersaturated solid-solution state in the matrix of the AZ61B precursor. Figure 5 shows the SEM-EDS analysis results of the precursor after the aging heat treatment at 200 °C for 86.4 ks in vacuum. Fine β -phases of less than $\sim 1 \mu\text{m}$ homogeneously existed as dispersoids in the α -Mg matrix as well as the coarse β -phases. This means that the α -Mg matrix of the precursor contained an excess of Al atoms. Fewer Al atoms could be solid-soluted in the α -Mg phase with a thermal stability below 200 °C.

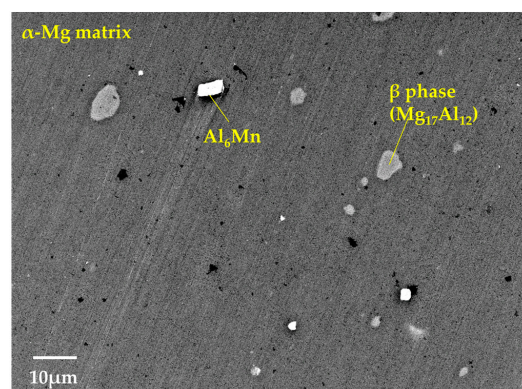
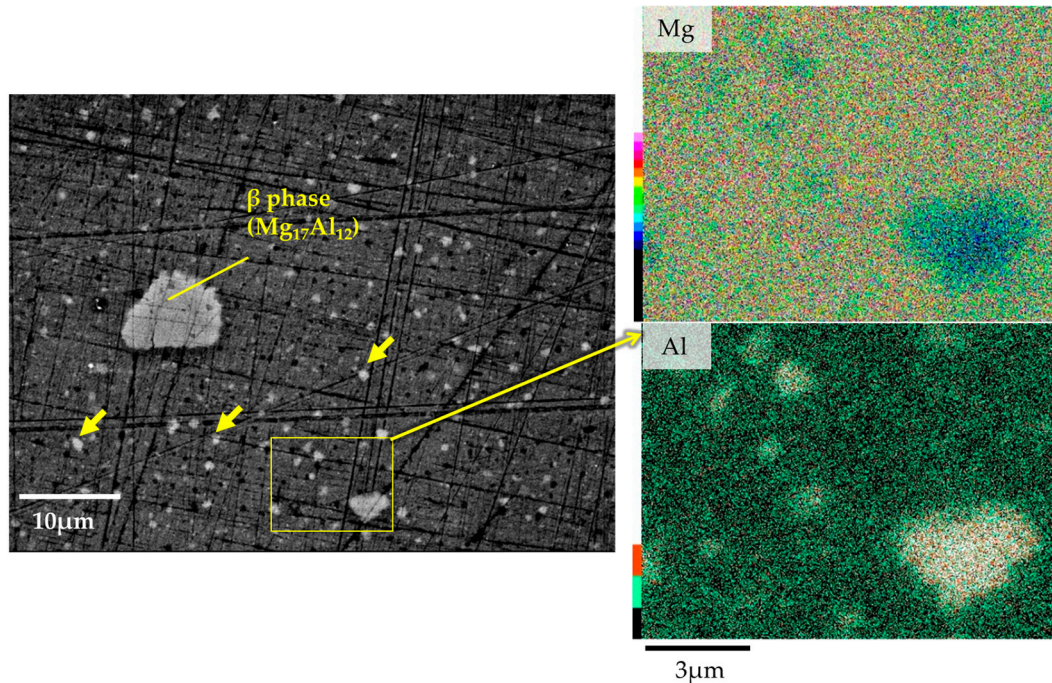


Figure 4. SEM observation on AZ61B powder precursor with no CaO particle after ECABMA process.

Table 1. Chemical compositions of the α -Mg matrix in AZ61B powder precursor with no CaO particle.

Element (at %)	Al	O	Zn	Mn	Mg	Total
α -Mg matrix	4.70	0.27	0.26	0.03	94.74	100.00

**Figure 5.** SEM-EDS analysis results of AZ61B powder precursor with no CaO particle after aging heat treatment at 200 °C for 86.4 ks in vacuum.

3.2. Microstructural Analysis on the α -Mg Phase of Mg–Al–CaO Precursors

Microstructural changes of the AZ61B composite precursor with 10-vol % CaO particles at the initial reaction stage were investigated by applying a heat treatment at 500 °C for 300 s. As shown in Figure 6a, the original CaO particles and in situ-formed intermediate precipitates observed using scanning transmission electron microscopy (STEM) were dispersed in the α -Mg polycrystalline matrix. Figure 6b shows a superposition of the TEM observation with an EDS mapping analysis on the α -Mg phase in the same sample at area A. The distributions of the Ca and Al elements were almost the same. Most elements were detected along the α -Mg grain boundaries. Figure 6c shows an electron diffraction pattern for the α -Mg phase at area B. Numerous MgO spots were detected. This is because the AZ61B chips had the original natural oxide surface films, and the additional oxidation of the AZ61B powder precursor occurred during the ECABMA process. Except for MgO and the α -Mg matrix, no other compound was detected. According to these results, it was concluded that Al and Ca atoms in Figure 6b were solid-soluted in the α -Mg matrix with no formation of Al–Ca compounds.

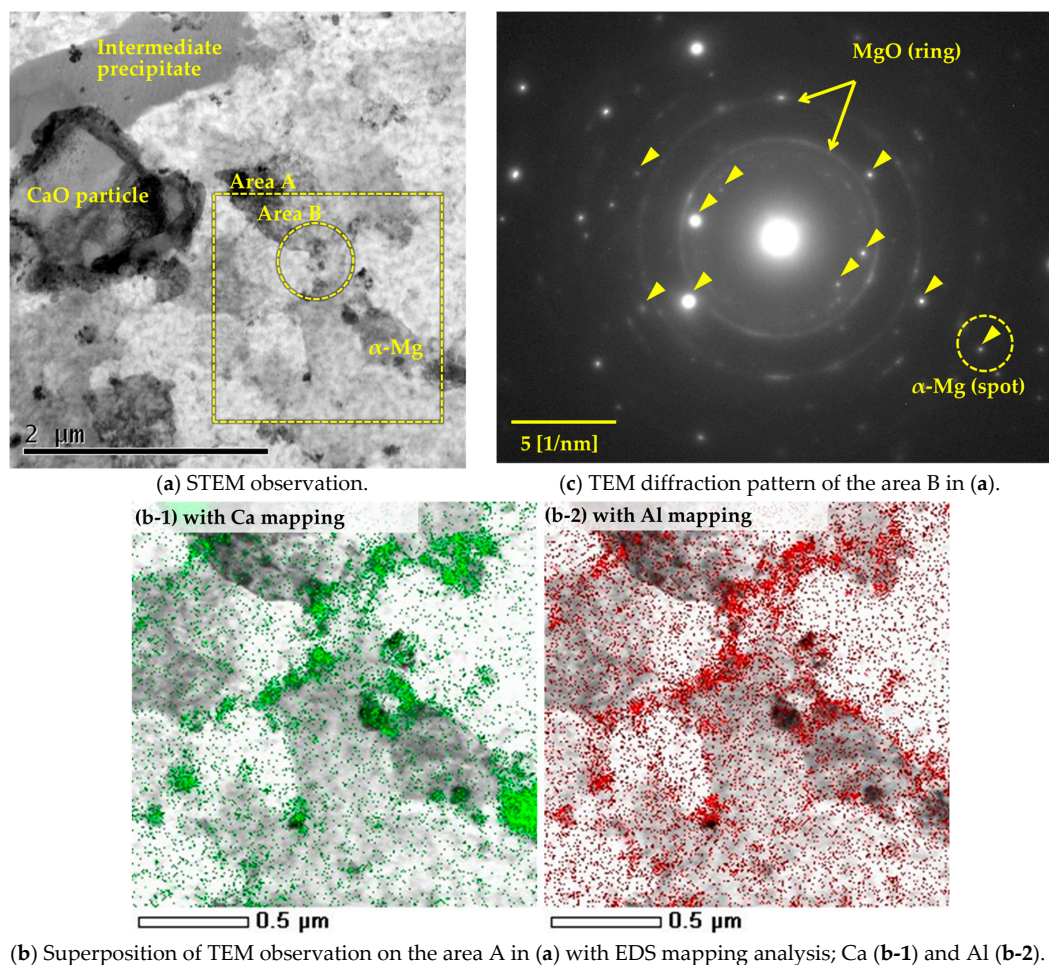


Figure 6. Transmission electron microscopy (TEM) observation result of the Mg–Al–CaO precursor with 10-vol % CaO particles after the heat treatment at 500 °C for 300 s. STEM: scanning transmission electron microscopy; EDS: energy-dispersive spectroscopy.

XRD analysis on the same precursor in the as-processed state (before heat treatment) and after the heat treatment at 500 °C for 300 s was carried out in order to investigate the crystal structure of α -Mg by solid solution. As shown in Figure 7, the XRD peak of the α -Mg phase in the as-processed state shifted to a higher angle compared to the original peak illustrated by the dotted line ($2\theta = 47.83^\circ$). This shift occurs because most of the Al atoms existed as a supersaturated solid-solution state in the α -Mg matrix of the as-processed precursor before heat treatment as mentioned in the previous section. Solid-soluted Al atoms created a smaller lattice spacing in α -Mg because the atomic radius of Al (1.43 Å) is smaller than that of Mg (1.60 Å) [16]. On the other hand, the same peak after the heat treatment at 500 °C for 300 s shifted to a lower angle. This is because the solid-soluted Al atoms in the α -Mg matrix decreased by forming intermediate precipitates containing Al and Ca as shown in Figure 6a and the previous study [12]. In addition, the XRD peak shifted to an even lower angle than the original α -Mg peak, as shown by the dotted line. This means that Ca atoms were also solid-soluted in the α -Mg matrix. The lattice spacing became larger than that of the original α -Mg because of the larger atomic radius of Ca (1.97 Å) compared to Mg (1.60 Å). Figure 8 shows an isothermal section of the Mg–Al–Ca ternary system in the Mg-rich corner at 450 °C [17]. It suggests that only a few of the Ca atoms are soluted in the α -Mg matrix, where the Al content is 4.7-at % as shown in Table 1. As a result, Ca atoms can be solid-soluted with thermal stability without Al–Ca precipitate formation when the Ca composition in the α -Mg matrix is within the solid solubility limit.

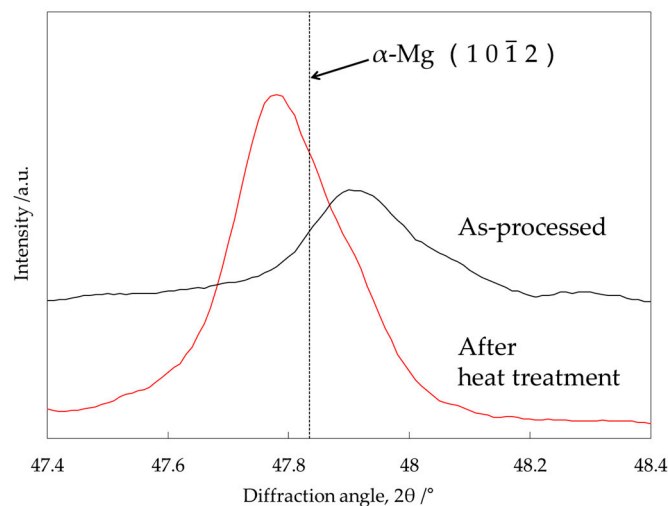


Figure 7. XRD patterns of the Mg–Al–CaO precursors with 10-vol % CaO particles in the as-processed state and after the heat treatment at 500 °C for 300 s.

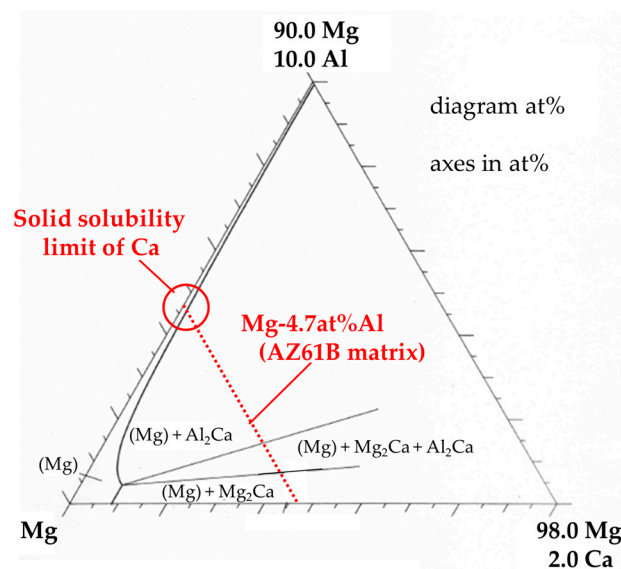


Figure 8. Isothermal section of the Mg–Al–Ca ternary system in Mg-rich corner at 450 °C.

According to the above consideration, when the heat treatment at 500 °C was applied to the Mg–Al–CaO precursor, CaO particles were thermally decomposed and Ca atoms were solid-soluted in the α -Mg matrix. Then, Ca atoms diffused along α -Mg grain boundaries as shown in Figure 6(b-1). Al atoms originally solid-soluted in the α -Mg matrix also diffused to the grain boundaries as displayed in Figure 6(b-2). This is because Al atoms were attracted to the Ca atoms due to a strong combination of Al and Ca elements [18]. As a result, the needle-like intermediate precipitates containing Al and Ca atoms were formed along the grain boundaries as shown in Figure 1.

Figure 9 shows TEM-EDS mapping analysis around a CaO particle of the precursor after the heat treatment at 500 °C for 300 s. MgO thin layers were observed around the CaO particle. They were formed by the solid-state reaction between oxygen atoms originated from CaO and Mg atoms in the α -Mg matrix. This suggests that both CaO reduction and Mg oxidation occurred at the interfacial

surface between CaO particles and the α -Mg matrix. In conclusion, the following reaction occurred in the precursor:



Based on the above consideration, it is expected that CaO reduction could occur in the Mg–Al alloy regardless of CaO content. However, our previous study [12] reported that no formation of an Al_2Ca phase was detected in a Mg–Al–CaO precursor with 2.5-vol % CaO particles as shown in Figure 2. This is possibly because a lower CaO content caused a smaller amount of Ca atoms to be solid-soluted in the matrix. This reaction behavior must be investigated in detail for situations of low CaO content.

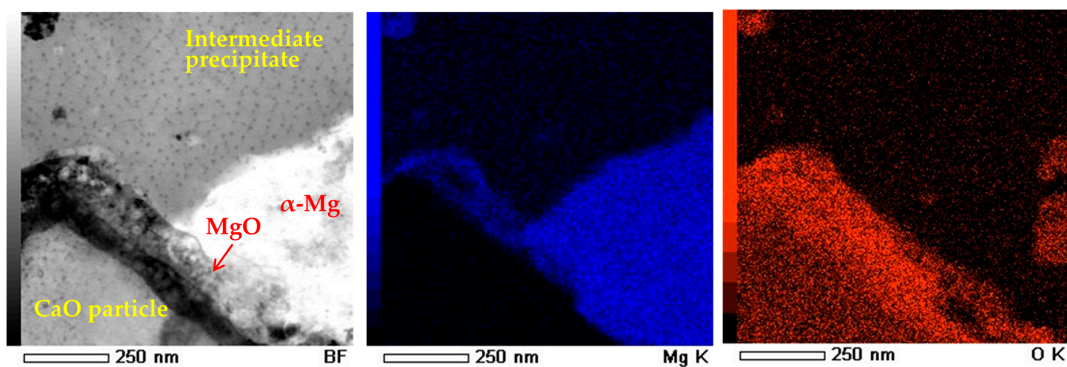


Figure 9. TEM-energy-dispersive spectroscopy (TEM-EDS) mapping analysis around CaO particle in the Mg–Al–CaO precursor with 10-vol % CaO particles after the heat treatment at 500 °C for 300 s.

3.3. Microstructural Analysis of the Intermediate Precipitates by TEM-EDS

As previously shown in Figure 1, the spherical Al_2Ca intermetallic precipitates were formed in the Mg–Al–CaO precursors with 10-vol % CaO particles after the heat treatment at 500 °C for 3.6 ks. On the other hand, a short heat treatment caused the formation of needle-like intermetallics as intermediate precipitates. Our previous study [12] reported that these intermediate compounds were detected as $(\text{Mg,Al})_2\text{Ca}$ or $\text{Al}_3\text{Ca}_4\text{Mg}$. However, the detailed structure was not completely identified. Therefore, a microstructural analysis of the intermediate precipitates was carried out. Figure 10a shows TEM-EDS line analysis results of an intermediate precipitate in the Mg–Al–CaO precursor with 10-vol % CaO particles after the heat treatment at 500 °C for 300 s. Mg, Al, and Ca were detected. Table 2 shows the chemical composition of this precipitate. The $(\text{Mg} + \text{Al})/\text{Ca}$ ratio was 2.09. Therefore, the intermediate precipitate was identified as $(\text{Mg,Al})_2\text{Ca}$. Figure 10b shows TEM observation and electron diffraction analysis on the precipitate. Rzychoń et al. [19] reported that a $(\text{Mg,Al})_2\text{Ca}$ Laves phase with a hexagonal C36 structure was formed in the Mg-5Al-3Ca-0.7Sr-0.2Mn alloy. Then, identification of the diffraction pattern in Figure 10(b-2) was determined by referring to the XRD pattern of $(\text{Mg,Al})_2\text{Ca}$ reported in the study [19]. Table 3 shows the referred XRD peak degrees of $(\text{Mg,Al})_2\text{Ca}$ and the lattice spacing calculated by the following Bragg reflection equation:

$$2d \sin \theta = n\lambda \quad (2)$$

where λ is the X-ray ($\text{Cu-K}\alpha$) wavelength of 1.5418 Å, n is the diffraction order of 1, and d is the lattice spacing. Diffraction spots indicated by the arrows in Figure 10(b-2) correspond to the lattice spacing of $(\text{Mg,Al})_2\text{Ca}$ according to the data of Table 3. As a result, this compound was identified as a $(\text{Mg,Al})_2\text{Ca}$ phase.

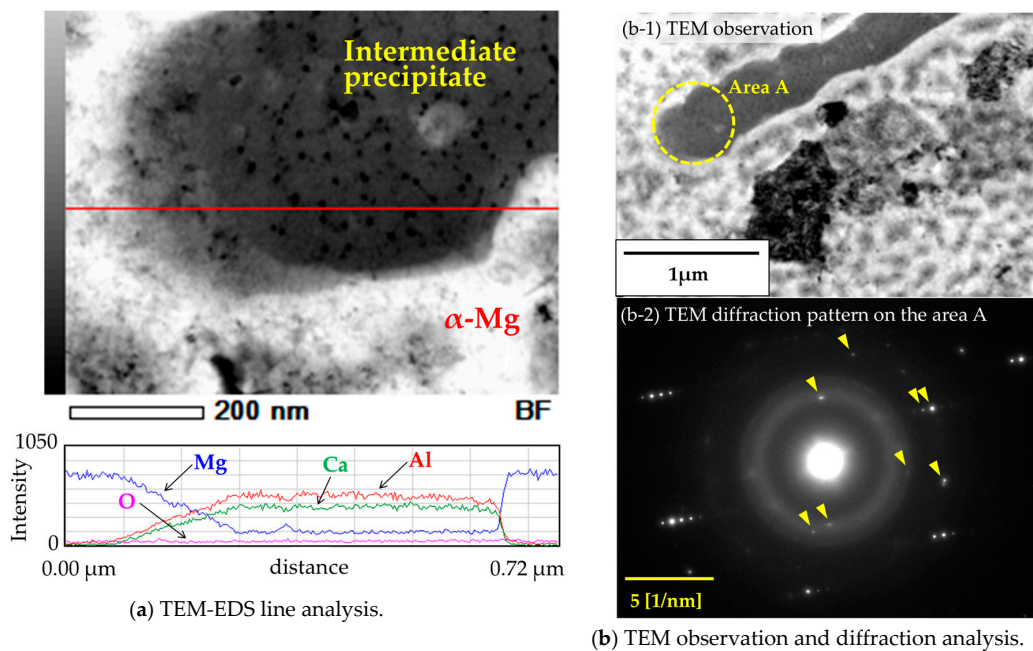


Figure 10. TEM observation on intermediate precipitate in the Mg–Al–CaO precursor with 10-vol % CaO particles after the heat treatment at 500 °C for 300 s.

Table 2. Chemical compositions of intermediate precipitates in the Mg–Al–CaO precursor with 10-vol % CaO particles after the heat treatment at 500 °C for 300 s.

Element (at %)	Mg	Al	Ca	O	Mn	Zn	Total
Intermediate precipitate	12.34	48.84	29.29	8.98	0.16	0.40	100.00

Table 3. (Mg,Al)₂Ca peak degrees of X-ray diffraction in Rzychoń’s work [19] and calculated lattice spacing from these peak degrees.

XRD Peak Degree, 2θ (°)	Calculated Lattice Spacing, d (Å)
29.44	3.033
30.65	2.916
33.53	2.673
38.20	2.356
43.01	2.103
49.54	1.840
56.80	1.621
61.57	1.506

3.4. Identification of the Intermediate Precipitates by XRD

In the above discussion, a phase identification was carried out by using only the XRD peak degrees (2θ) reported by Rzychoń et al. [19], which were limited within the range from 21° to 66°. In this section, XRD analysis was carried out in order to identify the same intermetallic precipitates by using the lattice spacing calculated from the lattice parameters of the (Mg,Al)₂Ca phase. Figure 11 shows the XRD profile of the Mg–Al–CaO precursor with 10-vol % CaO particles after the heat treatment at 500 °C for 300 s. The diffraction peaks indicated by triangles (▲) are estimated as the (Mg,Al)₂Ca compound. The diffraction angles indicated by diamonds (◆ and ◇) were calculated from the lattice spacing of (Mg,Al)₂Ca in the way described below.

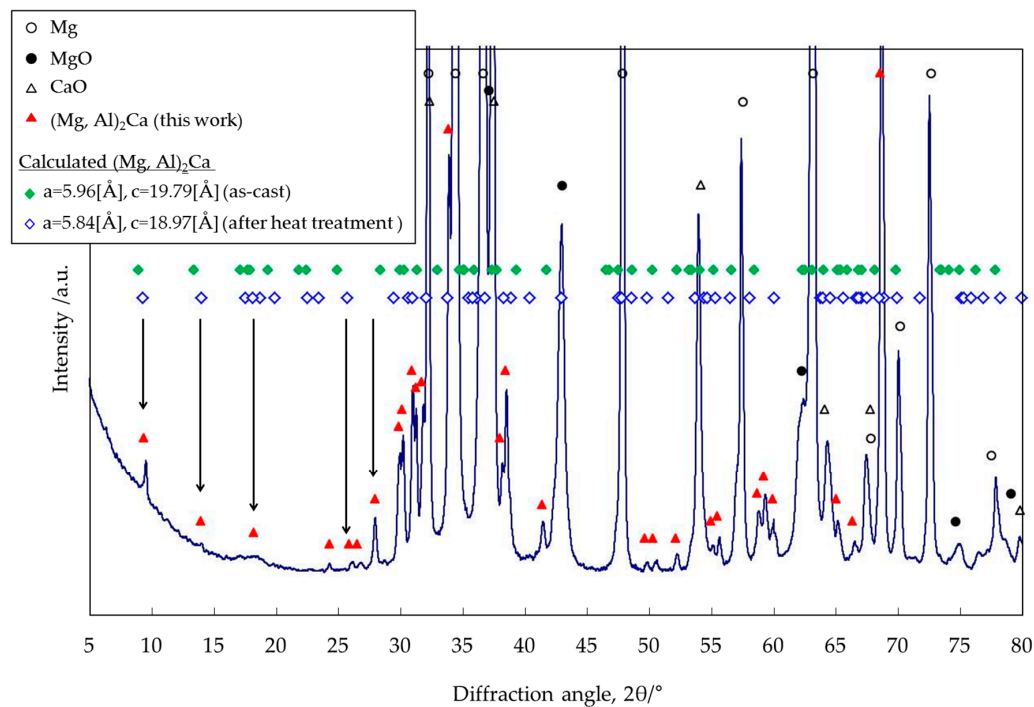


Figure 11. X-ray diffraction pattern of the Mg–Al–CaO precursor with 10-vol % CaO particles after the heat treatment at 500 °C for 300 s.

The lattice spacing (d_{hkl}) of the $(\text{Mg,Al})_2\text{Ca}$ phase can be calculated by the following Equation (3) because it has a hexagonal C36 structure:

$$\frac{1}{d_{hkl}} = \sqrt{\frac{4}{3} \frac{h^2 + hk + k^2}{a^2} + \frac{l^2}{c^2}} \quad (3)$$

where h , k , and l are the Miller indices, and a and c are the lattice parameters, respectively. Recently, many studies have reported that four kinds of Laves phases were formed in the Mg–Al–Ca system: Al_2Ca , Mg_2Ca , $(\text{Mg,Al})_2\text{Ca}$, and $\text{Al}_2(\text{Mg,Ca})$ [16,19–24]. The lattice parameters of the $(\text{Mg,Al})_2\text{Ca}$ and $\text{Al}_2(\text{Mg,Ca})$ phases have no specific value because of the variable compositions [16,24]. Suzuki et al. [16] reported that the $(\text{Mg,Al})_2\text{Ca}$ Laves phase was crystallized in the Mg–Al–Ca die-cast alloy with a C36 di-hexagonal structure, which was an intermediate between Mg_2Ca with a C14 hexagonal structure and Al_2Ca with a C15 cubic structure. According to the previous study [16], in the as-cast state, most of the Al atoms existed in the α -Mg matrix phase as a Mg–Al supersaturated solid-solution. Therefore, the crystal structure and composition of the $(\text{Mg,Al})_2\text{Ca}$ compound were close to the Mg_2Ca phase. On the other hand, after a heat treatment, both became close to the Al_2Ca phase because of the Al diffusion and substitution of Al for Mg in the α -Mg matrix contained in $(\text{Mg,Al})_2\text{Ca}$. Table 4 shows the lattice parameters of the $(\text{Mg,Al})_2\text{Ca}$ compound in the as-cast state and after a heat treatment referred from the previous study [16]. The lattice parameters after the heat treatment became smaller with an increase in the Al concentration of the $(\text{Mg,Al})_2\text{Ca}$ compound. This is because the atomic radius of Al (1.43 Å) is smaller than that of Mg (1.60 Å), as mentioned above.

Table 4. Crystal structures and lattice parameters of $(\text{Mg,Al})_2\text{Ca}$ Laves phases [16].

Compound	Type	Structure	Lattice Parameter	
			a (Å)	c (Å)
$(\text{Mg,Al})_2\text{Ca}$	C36	di-hexagonal (as-cast)	5.96	19.79
		di-hexagonal (after heat treatment)	5.84	18.97

Based on the above consideration, the lattice spacing of $(\text{Mg,Al})_2\text{Ca}$ was calculated from the two kinds of lattice parameters indicated in Table 4 by using Equation (3). After that, the XRD peak degrees were converted from the lattice spacing by Equation (2). Table 5 shows the calculated results. The Miller indices (h , k and l) were 0, 1, 2, 3, 4, and 5. The calculated values (2θ) are shown within the range from 0° to 80° . The XRD peak degrees calculated from both lattice parameters in Table 4 were similar. These values after the heat treatment were a little larger than those in the as-cast state due to the smaller lattice parameter. The calculated diffraction angles in the as-cast state and after the heat treatment are indicated by two kinds of diamonds (\blacklozenge and \blacklozenge), respectively, shown in Figure 11. Not all calculated peaks of the $(\text{Mg,Al})_2\text{Ca}$ Laves phase were detected because the calculated results in Table 5 included no information about their intensities. The diffraction peaks estimated as $(\text{Mg,Al})_2\text{Ca}$ (\blacktriangle) roughly correspond to those of the calculated ones (\blacklozenge and \blacklozenge). The low-angled peaks indicated by arrows matched them especially well. As a result, the intermediate compound was identified as the $(\text{Mg,Al})_2\text{Ca}$ Laves phase. In addition, the detected peaks at $\sim 9.5^\circ$ and $\sim 14^\circ$ correspond to the calculated ones for after the heat treatment rather than those of the as-cast state. According to the above analysis and discussion, this suggests that the crystal structure and compositions of the intermediate compound are closer to Al_2Ca than they are to Mg_2Ca . This also agrees with the result showing that the Al content of the compound was much higher than the Mg content as shown in Table 2. It is expected that the crystal structure of the intermediate precipitate becomes much closer to that of Al_2Ca when a long heat treatment is employed. This is because Al atoms in the α -Mg matrix are substituted for Mg atoms contained in $(\text{Mg,Al})_2\text{Ca}$. As a result, Al_2Ca compounds were homogeneously dispersed after the heat treatment for 3.6 ks as shown in Figure 1. Their shapes became spherical in order to reduce the surface energy.

Table 5. Miller indices and calculated diffraction angles of $(\text{Mg,Al})_2\text{Ca}$ Laves phase.

Miller Indices				Diffraction Angle, 2θ ($^\circ$)		Miller Indices				Diffraction Angle, 2θ ($^\circ$)	
h	k	i	l	As-Cast ($a = 5.96(\text{\AA})$) ($c = 19.79(\text{\AA})$)	After Heat Treatment ($a = 5.84(\text{\AA})$) ($c = 18.97(\text{\AA})$)	h	k	i	l	As-Cast ($a = 5.96(\text{\AA})$) ($c = 19.79(\text{\AA})$)	After Heat Treatment ($a = 5.84(\text{\AA})$) ($c = 18.97(\text{\AA})$)
0	0	0	1	4.46	4.66	2	1	-3	4	50.27	51.55
0	0	0	2	8.94	9.32	2	1	-3	5	52.28	53.69
0	0	0	3	13.42	14.01	3	0	-3	0	53.24	54.42
1	0	-1	0	17.18	17.53	3	0	-3	1	53.46	54.65
1	0	-1	1	17.76	18.15	3	0	-3	2	54.10	55.35
0	0	0	4	17.93	18.71	3	0	-3	3	55.17	56.49
1	0	-1	2	19.40	19.89	3	0	-3	4	56.64	58.07
1	0	-1	3	21.86	22.51	3	0	-3	5	58.49	60.05
0	0	0	5	22.46	23.45	2	2	-4	0	62.31	63.74
1	0	-1	4	24.93	25.75	2	2	-4	1	62.51	63.95
1	0	-1	5	28.42	29.43	2	2	-4	2	63.10	64.58
1	1	-2	0	29.98	30.62	2	2	-4	3	64.07	65.63
1	1	-2	1	30.33	30.99	3	1	-4	0	65.16	66.68
1	1	-2	2	31.35	32.07	3	1	-4	1	65.36	66.88
1	1	-2	3	32.98	33.81	2	2	-4	4	65.41	67.07
2	0	-2	0	34.76	35.50	3	1	-4	2	65.93	67.50
2	0	-2	1	35.06	35.82	3	1	-4	3	66.88	68.52
1	1	-2	4	35.15	36.12	2	2	-4	5	67.12	68.91
2	0	-2	2	35.96	36.78	3	1	-4	4	68.19	69.93
2	0	-2	3	37.42	38.33	3	1	-4	5	69.87	71.74
1	1	-2	5	37.79	38.92	4	0	-4	0	73.37	75.14
2	0	-2	4	39.38	40.42	4	0	-4	1	73.55	75.33
2	0	-2	5	41.78	42.98	4	0	-4	2	74.10	75.92
2	1	-3	0	46.55	47.57	4	0	-4	3	75.00	76.89
2	1	-3	1	46.79	47.82	4	0	-4	4	76.25	78.25
2	1	-3	2	47.50	48.58	4	0	-4	5	77.86	79.98
2	1	-3	3	48.67	49.83	-	-	-	-	-	-

4. Conclusions

AZ61B composite powder precursors with 10-vol % CaO additive particles prepared via the ECABMA process were heat treated to synthesize Al_2Ca intermetallic precipitates in a solid-state reaction. SEM-EDS and EPMA were applied to investigate the distribution of Al atoms in the AZ61B powder precursor. The precursor before the heat treatment indicated that the α -Mg matrix contained 4.7-at % Al atoms and the remaining Al elements contributed to forming $\text{Mg}_{17}\text{Al}_{12}$ or Al_6Mn compounds in the matrix. TEM-EDS and XRD analysis on the AZ61B composite precursor in the initial reaction stage showed that CaO additives were thermally decomposed in the Mg–Al alloy matrix, and solid-soluted Ca atoms diffused along the α -Mg grain boundaries. Al atoms also diffused to the grain boundaries because of their strong affinity for Ca atoms. As a result, needle-like $(\text{Mg,Al})_2\text{Ca}$ intermetallics were formed as intermediate precipitates at the initial stage of the heat treatment. They were completely transformed into the spherical Al_2Ca phases by substitution of Al atoms for Mg atoms of the above $(\text{Mg,Al})_2\text{Ca}$ intermediates after a long heat treatment.

Acknowledgments: The authors would like to thank Keitaro Enami, Masaki Ohara, Takanori Igarashi from TOPY Industries, Limited, for supporting preparation of AZ61B precursors containing CaO particles via ECABMA process.

Author Contributions: Junji Fujita and Katsuyoshi Kondoh conceived and designed the experiments. Junji Fujita performed the experiments. Junji Fujita and Junko Umeda analyzed the results. Junji Fujita wrote the paper. Junko Umeda and Katsuyoshi Kondoh supervised the experiments and the paper.

Conflicts of Interest: The authors declare no conflict of interest.

References

1. Gupta, M.; Sharon, N.M.L. *Magnesium, Magnesium Alloys, and Magnesium Composites*; John Wiley & Sons: Hoboken, NJ, USA, 2011.
2. U.S. Geological Survey. *Mineral Commodity Summaries*; U.S. Geological Survey: Reston, VA, USA, 2015.
3. Tharumarajah, A.; Koltun, P. Is there an environmental advantage of using magnesium components for light-weighting cars? *J. Clean. Prod.* **2007**, *15*, 1007–1013. [[CrossRef](#)]
4. Luo, A.A. Magnesium casting technology for structural applications. *J. Magnes. Alloys* **2013**, *1*, 2–22. [[CrossRef](#)]
5. Bettles, C.J.; Gibson, M.A.; Zhu, S.M. Microstructure and mechanical behaviour of an elevated temperature Mg-rare earth based alloy. *Mater. Sci. Eng. A* **2009**, *505*, 6–12. [[CrossRef](#)]
6. Pekguleryuz, M.O.; Kaya, A.A. Creep resistant magnesium alloys for powertrain applications. *Adv. Eng. Mater.* **2003**, *5*, 866–878. [[CrossRef](#)]
7. Anyanwu, I.A.; Gokan, Y.; Suzuki, A.; Kamado, S.; Kojima, Y.; Takeda, S.; Ishida, T. Effect of substituting cerium-rich mischmetal with lanthanum on high temperature properties of die-cast Mg–Zn–Al–Ca–RE alloys. *Mater. Sci. Eng. A* **2004**, *380*, 93–99. [[CrossRef](#)]
8. Amberger, D.; Eisenlohr, P.; Göken, M. Microstructural evolution during creep of Ca-containing AZ91. *Mater. Sci. Eng. A* **2009**, *510*, 398–402. [[CrossRef](#)]
9. Kondori, B.; Mahmudi, R. Effect of Ca additions on the microstructure, thermal stability and mechanical properties of a cast AM60 magnesium alloy. *Mater. Sci. Eng. A* **2010**, *527*, 2014–2021. [[CrossRef](#)]
10. Xu, S.W.; Matsumoto, N.; Yamamoto, K.; Kamado, S.; Honma, T.; Kojima, Y. High temperature tensile properties of as-cast Mg–Al–Ca alloys. *Mater. Sci. Eng. A* **2009**, *509*, 105–110. [[CrossRef](#)]
11. Ellingham, H.J.T. The physical chemistry of process metallurgy. *J. Soc. Chem. Ind.* **1944**, *63*, 125–133.
12. Kondoh, K.; Fujita, J.; Umeda, J.; Imai, H.; Enami, K.; Ohara, M.; Igarashi, T. Thermo-dynamic analysis on solid-state reduction of CaO particles dispersed in Mg–Al alloy. *Mater. Chem. Phys.* **2011**, *129*, 631–640. [[CrossRef](#)]
13. Enami, K.; Ohara, M.; Igarashi, T.; Fujita, J.; Kondoh, K. Development of Heat-Resistant Magnesium Composites by Bulk Mechanical Alloying Method. *J. Jpn. Soc. Powder Powder Metall.* **2009**, *56*, 717–721. (In Japanese) [[CrossRef](#)]

14. Enami, K.; Fujita, Y.; Motoe, Y.; Ohara, M.; Igarashi, T.; Kondoh, K. Development of magnesium alloy composites by bulk mechanical alloying process. *J. Jpn. Soc. Powder Metall.* **2008**, *55*, 244–249. (In Japanese) [[CrossRef](#)]
15. Massalski, T.B. *Binary Alloy Phase Diagrams*; American Society for Metals: Metals Park, OH, USA, 1986; Volume 1.
16. Suzuki, A.; Saddock, N.D.; Jones, J.W.; Pollock, T.M. Structure and transition of eutectic (Mg,Al)₂Ca Laves phase in a die-cast Mg–Al–Ca base alloy. *Scr. Mater.* **2004**, *51*, 1005–1010. [[CrossRef](#)]
17. Petzow, G.; Effenberg, G. *Ternary Alloys, A Comprehensive Compendium of Evaluated Constitutional Data and Phase Diagrams*; Verlagsgesellschaft: Weinheim, Germany, 1990; Volume 3, p. 614.
18. Nakaura, Y.; Watanabe, A.; Otori, K. Effects of Ca, Sr Additions on Properties of Mg–Al Based Alloys. *Mater. Trans.* **2006**, *47*, 1031–1039. [[CrossRef](#)]
19. Rzychoń, T.; Chmiela, B. The influence of tin on the microstructure and creep properties of a Mg-5Al-3Ca-0.7Sr-0.2Mn magnesium alloy. *Solid State Phenom.* **2012**, *191*, 151–158. [[CrossRef](#)]
20. Suzuki, A.; Saddock, N.D.; Jones, J.W.; Pollock, T.M. Solidification paths and eutectic intermetallic phases in Mg–Al–Ca ternary alloys. *Acta Mater.* **2005**, *53*, 2823–2834. [[CrossRef](#)]
21. Zhong, Y.; Liu, J.; Witt, R.A.; Sohn, Y.; Liu, Z. Al₂(Mg,Ca) phases in Mg–Al–Ca ternary system: First-principles prediction and experimental identification. *Scr. Mater.* **2006**, *55*, 573–576. [[CrossRef](#)]
22. Suzuki, A.; Saddock, N.D.; Jones, J.W.; Pollock, T.M. Phase Equilibria in the Mg–Al–Ca Ternary System at 773 and 673 K. *Metall. Mater. Trans. A* **2006**, *37*, 975–976. [[CrossRef](#)]
23. Janz, A.; Grobner, J.; Cao, H.; Zhu, J.; Chang, Y.A.; Schmid-Fetzer, R. Thermodynamic modeling of the Mg–Al–Ca system. *Acta Mater.* **2009**, *57*, 682–694. [[CrossRef](#)]
24. Kevorkov, D.; Medraj, M.; Li, J.; Essadiqi, E.; Chartrand, P. The 400 °C isothermal section of the Mg–Al–Ca system. *Intermetallics* **2010**, *18*, 1498–1506. [[CrossRef](#)]



© 2017 by the authors. Licensee MDPI, Basel, Switzerland. This article is an open access article distributed under the terms and conditions of the Creative Commons Attribution (CC BY) license (<http://creativecommons.org/licenses/by/4.0/>).